Technical feasibility of microwave absorbers for straylight mitigation in the LiteBIRD MHFT telescopes

Andrea Occhiuzzi[a, b, c], Gangapreet Singh[d], Elia Battistelli[a, b], Paolo de Bernardis[a, b], Federico Cacciotti[a, b], Fabio Columbro[a, b], Alessandro Coppolecchia[a, b], Giuseppe D'Alessandro[a, b], Marco De Petris[a, b], Jon E. Gudmundsson[d,f], Luca Lamagna[a, b], Elisabetta Marchitelli[a, b], Silvia Masi[a, b], Silvia Micheli[a, b], Mara Moriconi[a], Alessandro Novelli[a, b, c], Alessandro Paiella[a, b], Francesco Piacentini[a, b], Giampaolo Pisano[a, b], Giorgio Savini[e], and Alexei Shitvov[e], for the LiteBIRD Collaboration[g]

[a]Dipartimento di Fisica, Sapienza Università di Roma, P.le A. Moro 5, 00185, Roma, Italy
[b]INFN–Sezione di Roma1, P.le A. Moro 5, 00185, Roma, Italy
[c]Dipartimento di Fisica, Università di Roma Tor Vergata, Via della Ricerca Scientifica 1, 00133, Roma, Italy
[d]The Oskar Klein Centre, Department of Physics, Stockholm University, AlbaNova, SE-10691 Stockholm, Sweden
[e]Physics and Astronomy Dept., University College London (UCL), London, UK
[f]Science Institute, University of Iceland, 107 Reykjavik, Iceland
[g]LiteBIRD Collaboration Members are listed at this link

ABSTRACT

The *LiteBIRD* mission is dedicated to the search for primordial *B* modes in the Cosmic Microwave Background (CMB) polarization. To achieve unprecedented sensitivity and accuracy in this measurement, the control of instrument systematics is paramount. In this context, we describe the development of microwave absorbers needed to mitigate the straylight within the telescope tubes of the *LiteBIRD* Mid- and High-Frequency Telescopes (MHFT). A baseline solution has been designed and validated using HFSS simulations, consistently demonstrating sub-percent level specular reflectance across the entire 90-448 GHz band of the MHFT under a broad variety of incidence conditions, representative of the actual optical environment predicted for the two telescopes. Leveraging consolidated technologies, a prototype has been manufactured and characterized in laboratory, demonstrating a promising reflectance mitigation despite the deviation from the nominal geometry. Ongoing parallel efforts involve a comprehensive investigation (both through simulations and laboratory measurements) of the requirements to be finalized in order to define the practical implementation of the baseline design. This activity will ultimately ensure the alignment with allocated thermo-mechanical requirements along with the compliance with the desired electromagnetic performance. The presented studies not only solidify the feasibility of the straylight mitigation approach, but also inform the finalization of the optical tube design, in view of the conclusion of the CNES Phase A study of *LiteBIRD*.

Keywords: *LiteBIRD*, microwave absorbers, anti-reflection coating, straylight, refractive index, loss tangent.

1. INTRODUCTION

The search for the *B* modes of the Cosmic Microwave Background polarization represents one of the most challenging tasks in observational cosmology. The *B* modes signal is extremely faint and is overwhelmed by various contamination sources, including foregrounds, gravitational lensing and instrumental systematics. To distinguish the scientific signal from the contamination, the *LiteBIRD*[1] experiment required the monitoring of polarized foregrounds thanks to a wide spectral coverage and the implementation of an optimized design and

---

Further author information: (Send correspondence to A. Occhiuzzi)
A. Occhiuzzi: E-mail: andrea.occhiuzzi@roma1.infn.it, Telephone: +39-6-49914201

accurate calibration to control systematic effects.

To achieve the large spectral coverage, the *LiteBIRD* instrument is composed of three telescopes: the Crossed-Dragone Low-frequency Telescope (LFT) and the two refractive Mid-Frequency Telescope (MFT) and High-frequency Telescope (HFT). In particular, for the Mid- and High-frequency Telescope (MHFT), a study of the straylight propagation in the telescope tubes shows that this is one of the most critical instrumental systematics. An optical design that minimizes this phenomenon is fundamental in order to avoid the formation of optical ghosts on the focal plane and leakage of E modes into B modes in the reconstructed sky maps.

An in-depth study about the ray-tracing propagation of straylight and impact on the focal plane is reported in [2]. The most effective solution to mitigate straylight is the incorporation of a microwave absorbing layer on the internal surfaces of the optical tubes. The constraints on weight and volume due to limited resource allocation of the payload require the development of a lightweight and compact absorber solution, suitable for cryogenic operation (the MHFT optics tubes are expected to operate at 4K) and qualified or qualifable for space applications.

Lossy dielectrics have been commonly used as reference blackbody targets or microwave absorbers in different microwave applications, including CMB experiments (e.g. COBE FIRAS[3] and Simon Observatory[4]). The base material is typically an epoxy resin, which is usually mixed with loading materials, such as carbon black, alumina, ceramic spheres, and so forth, in order to enhance the absorbance and to align the thermal coefficient of expansion with that of the substrate material.[5–7]

Given the ambitious observational target of *LiteBIRD*, the development of a suitable absorber prototype must take into account a proper characterization and modeling campaign to ensure that the optical performance is consistent with the mission requirements. Following a consolidated design, a prototype is constructed using a double mold technique. The optical properties are tested over a wide range of frequencies and incidence angles by using a differential Fourier Transform Spectrometer with a Martin-Puplett design (DFTS).[8,9] Additionally, an independent coherent setup is employed to measure the specular and diffuse reflectance of the samples. The discrepancy between the observed and expected performance was investigated through refined simulations using Ansys HFSS.

In this paper, we first present the design and the simulations for a baseline design suitable for prototyping (Sect. 2). We then present the manufacturing process and imaging of the fabricated samples performed with a scanning electron microscope (Sect. 3) and finally we present the results of the optical tests performed with two independent measurement setups (Sect. 4).

2. DESIGN AND SIMULATION

The current feasibility study on the *LiteBIRD* MHFT absorbers is focused on the identification of a suitable and space-qualified design and recipe. In order to achieve a high absorption capacity while maintaining a thin thickness due to space and weight constraints, a high-loss material is required. The generally much higher refractive index of one of these materials produces an impedance mismatch between the free space and the bulk, which results in the reflection of some of the incident radiation.

While waiting for an assessed requirement on the reflectance level, our study consider a baseline of 1 % reflectance for the absorbers, as this ensures an optimal suppression of straylight propagation in the tube. The reduction of reflectance in an optical device can be achieved through a number of different anti-reflection coatings (ARCs).[10] One such approach is the use of three-dimensional structures patterned on the first surface, such as pyramids, which ensures a number of advantages.[11] Depending on the frequency band and the dimensions of the pyramids, this ARC can act both as an impedance matching from the vacuum to the bulk, thanks to the smooth transition of the mean refractive index at low frequency, and as a "light trap" at higher frequencies, where multiple, inefficient reflections may take place against different facets of the structure. The effectiveness of reflection suppression is strongly dependent on the shape and the aspect ratio of the pyramids. The choice of the design of our prototype is driven by the need to achieve a reflectance below 1 % across the entire frequency band of MHFT (90 GHz-448 GHz).

The anti-reflection coating design uses a square-based pyramid structure with a side length of 0.6 mm and a height of 1.5 mm. While the geometry is similar to the one presented in [12], the bulk absorber and the manufacturing process for our prototype are different: in our case, an epoxy-based, lossy mixture is used, which sets constraints
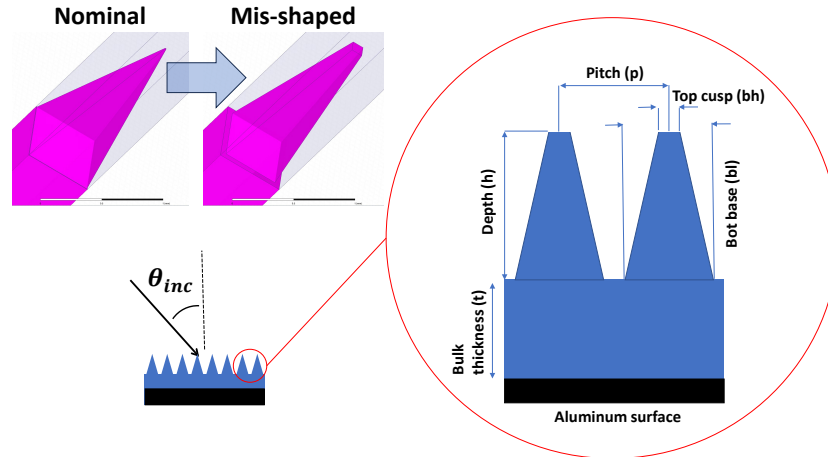
Figure 1. A scheme of the pyramidal nominal geometry and the mis-shape design used to simulate the actual prototype performance. The rounding of the pyramid tip and the filling of the through at the base are taken into account in the mis-shaped design.

in terms of curing temperature and times, and ultimately limits the possibility to produce samples by injection-molding.

The model is validated through a HFSS simulation of a periodic-cell absorbing plate, which is tested for different incidence angles and polarization states of the incoming radiation. The structure is excited through a couple of bi-moded Floquet ports, where the two fundamental Floquet modes correspond to linearly polarized plane waves, and the dielectric constant and loss tangent of the bulk absorber are matched to the values measured in the lab (see Sect.4).

A simple S-matrix analysis provides the necessary prediction for the reflectance. In order to compare the simulation with the experimental results, the simulated structure is a bulk slab of 4 mm thickness, with pyramid structure on one face only. Additional iterations of the same design have been simulated to include anti-reflection treatment on both faces or to reproduce the presence of a conducting surface on the opposite side, but all the results are dominated by the residual mismatch on the first interface, since the dielectric loss through the bulk is sufficiently high to suppress most of the additional contribution from round-trip radiation from the second interface. In the following, we show and discuss in particular the simulations of the single-face structure with direct coupling to vacuum on the flat side, as in the measurements of the prototypes. The results of the simulation are presented in Fig. 2.

 Furthermore, a simple simulation of the performance degradation was run, incorporating a non-ideal shape of the pyramids that arises during the manufacturing process. The systematic errors introduced in the simulations are the fixed truncation of the pyramid tips and a progressive filling of the troughs at the base. The overall degradation of performance observed in the simulation is in agreement with the measured degradation of the prototype. However, we do not expect to be able to fully reproduce the actual performance through this approach, since the periodic cell in the simulation implements a systematic deviation with no statistical variability across a surface of finite extension (see Sect. 3).

3. PROTOTYPE MANUFACTURING

The definition of a manufacturing process that guarantees high reproducibility and low deviations from the ideal ARC design is a key point in our study on *LiteBIRD* absorbers. In order to facilitate future collaboration with industrial manufacturers in view of mass production, a preliminary production process was established for the purpose of studying the optical properties of different material mixtures, the performance of the ARC design and the tolerance with respect to the deviation of the pyramids from the nominal shape.
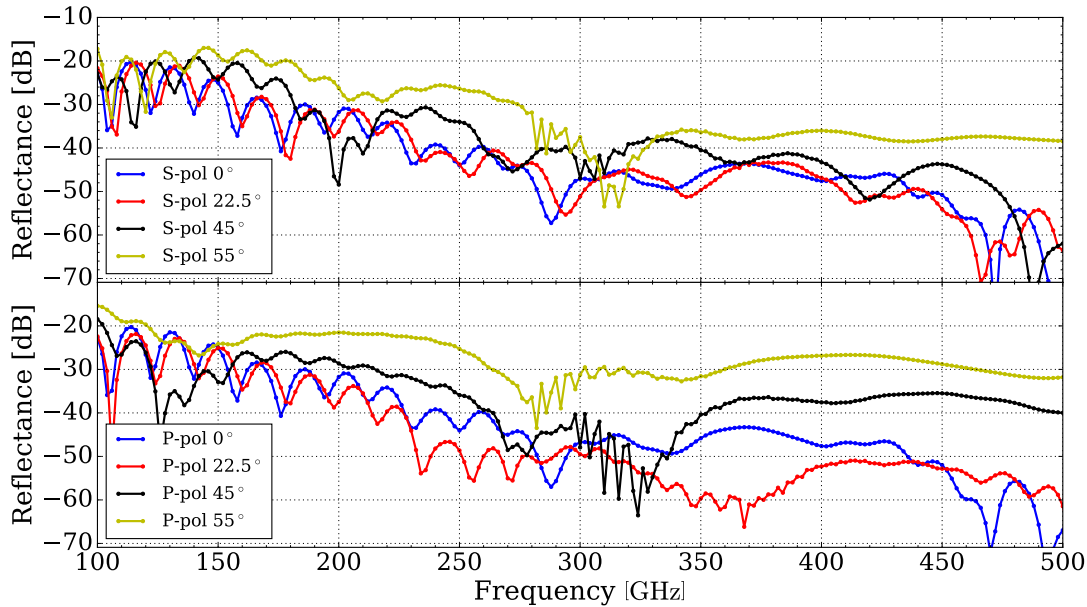
Figure 2. Simulated reflectance for the nominal pyramid geometry at incidence angles of 0°, 22.5°, 45° and 55° for the S-Pol (upper panel) and the P-Pol (lower panel). The anti-reflection coating performance declines as the angle of incidence increases, yet remains below the 1% threshold.
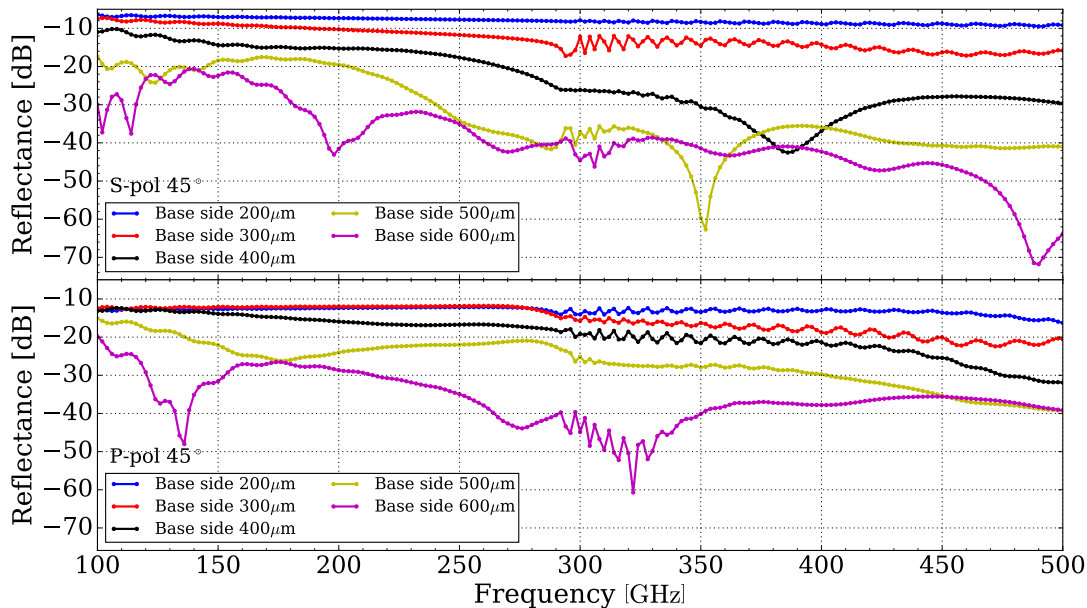

Figure 3. Simulated reflectance for the mis-shaped pyramid geometry at incidence angles of 45° for the S-Pol (upper panel) and the P-Pol (lower panel). The dimensions of the pyramids base side are reduced by a step of 100 μm, while the angle at the edge is conserved, resulting in a progressive diminution of the pyramids height and an increasing of the filling of the troughs at the base.

Two epoxy resins have been selected as the base material: Eccosorb CR110[*] and STYCAST 2850FT[†]. The rationale behind this choice is that both resins have already been used in other space environments and are highly

---

[*]https://www.laird.com/products/absorbers/structural-absorbers/castable-liquid-absorber/eccosorb-cr
[†]https://www.henkel-adhesives.com/it/it/prodotto/potting-compounds/loctite_stycast_2850ftblk.html

lossy. The Eccosorb CR110 is initially employed to fabricate flat plates as a preliminary test for the measurements of transmittance, reflectance and refractive index with our setup. It is no longer used for the subsequent prototypes due to the presence of ferromagnetic powder within the resin, which can induce an unpredictable behaviour in the presence of a strong magnetic field, such as that of the polarization modulator unit.[13,14] The recipe incorporates carbon black dust with a grain size of $10\,\mu m - 250\,\mu m$ as loading material, with the objective of enhancing the dielectric loss. These recipes are expected to be modified with the addition of silica powder or alumina, with the objective of reducing the build-up of mechanical stress during cooldown by adapting the thermal expansion coefficient to that of the aluminum substrate.

The manufacturing process comprises three stages: the production of a positive mold using a 3D printer, the
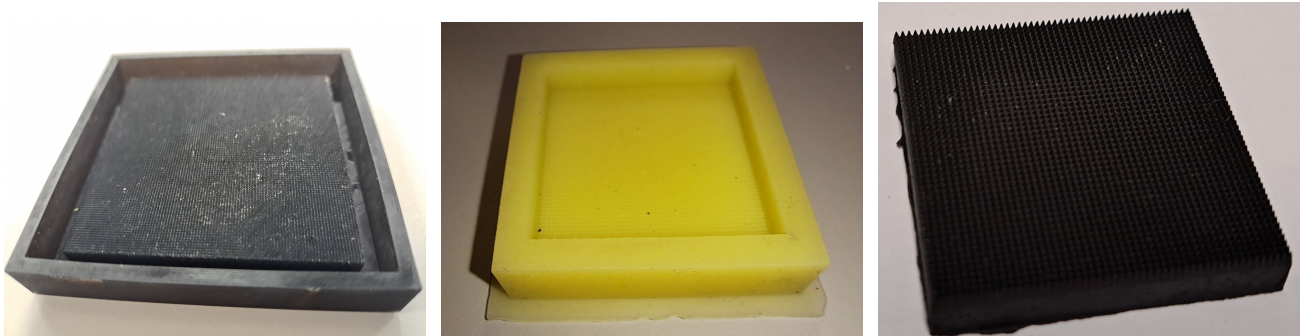

Figure 4. The three stages of the manufacturing process: on the left is the first positive 3D printed master, in the center is the silicone negative mold and on the right is the actual prototype.

production of a negative silicone mold from the 3D-printed master, and the actual prototype production by pouring the lossy resin into the silicone mold (see Fig.4). The positive master is produced with an ultraviolet (UV) printer to ensure the highest spatial fidelity among the available consumer-level 3D printing technologies. The negative mold is produced using a commercial two-component silicone, which is first vigorously mixed for $2 - 3\,min$ and out-gassed for approximately $15\,min$ in a vacuum chamber at a pressure below $\sim 10\,mbar$. Subsequently, the silicone is poured into the mold and a second out-gassing is performed for $10 - 20\,min$. Finally, the silicone is cured at $65\,°C$ for $3\,h$.

The production of the actual absorber prototype begins with the preparation of the loaded epoxy resin mixture. The first phase is to mix the resin with the hardener and then gradually add the chosen percentage by weight of carbon powder, then mixing until a homogeneous mixture is obtained. Out-gassing is performed with the same methodology employed for the silicone, extending the duration of the process until no significant residual activity is observed. The curing of the resin is conducted at a temperature of $65\,°C$ for $13\,h$. The detachment from the mold require the deposition of a layer of silicon-free detaching wax prior to the mixture pouring. This step is believed to affect the accuracy in the replication of the surface features, ultimately limiting the measured performance with respect to the nominal geometry. An alternative solution for mold detachment is under investigation to improve the final quality of the molded geometry.

The imaging of the prototype is performed using a scanning electron microscope (SEM) as shown in Fig.5. As anticipated, we observe a non-negligible deviation of the average pyramidal profile from the nominal model and a filling of troughs at the pyramid base by $\sim 280\,\mu m$. A systematic truncation of the pyramid tips by $\sim 250\,\mu m$ and an overall reduction of the height of $\sim 300\,\mu m$ is also observed, resulting in the total height being on average $300 - 500\,\mu m$ lower than expected. Re-simulation of the performance with a similar geometry yielded (see Fig. 3) results more consistent with the measurements, even if the periodic cell approach does not allow to reproduce the statistical distribution of geometry deviations, ultimately limiting the fidelity of the simulations.

4. TEST RESULTS

The optical properties of the loaded resins are measured using a Differential Fourier Transform Spectrometer based on a Martin-Puplett design.[9] A custom-designed multi-mirror optical system allows to perform transmittance and reflectance measurements for a broad range of incidence angles: $-70° < \theta < 70°$ in transmission,
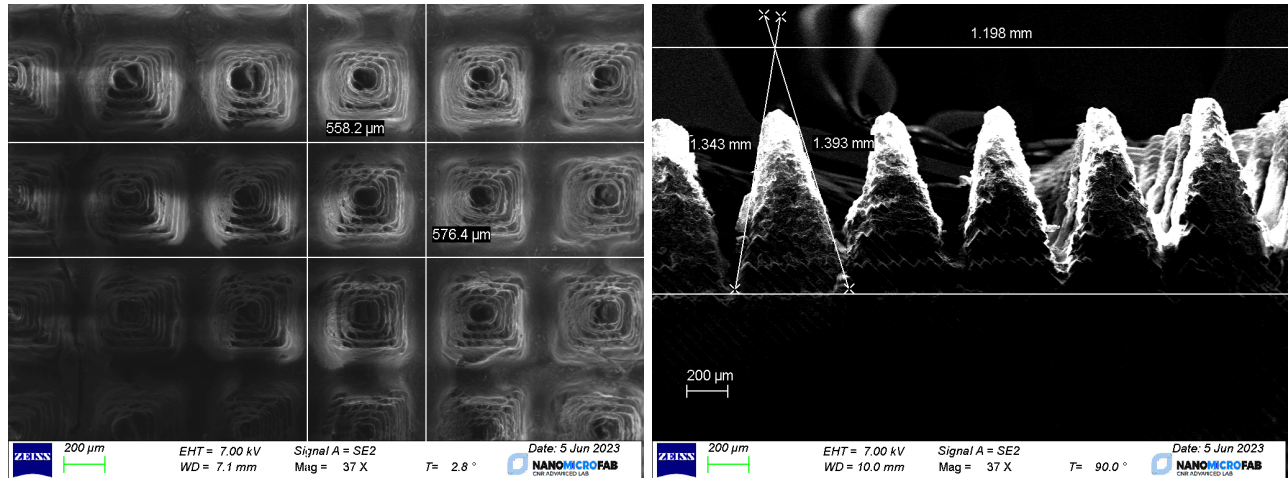
Figure 5. SEM photographs of a carbon loaded STYCAST 2850FT prototype. Left: from the top view, a deviation from the expected size of the pyramid side, corresponding to approximately 40 µm, and a general filling at the pyramids base was observed. Right: from the side view, an overall reduction of 300 µm in the height of the pyramid and a truncation of the tips of approximately 250 µm was shown.

$45° < \theta < 70°$ and $22.5°$ in reflection. An anti-aliasing low-pass filter with a cut-off frequency of 480 GHz is employed to ensure the out-of-band rejection $(100\,\text{GHz} - 500\,\text{GHz})$ and to enhance the signal-to-noise ratio (S/N) at low frequencies. The two input ports are filled with a mercury arc lamp at an effective temperature of 3000 K and an Eccosorb HR10 panel at 300 K respectively. The signal is modulated with a chopper at a frequency of 33 Hz and then demodulated with a Lock-in Amplifier.

Interferograms are scanned and collected through a standard step-and-integrate approach. This involves acquiring the signal for each position of the movable mirror after a minimum integration time of $10\times$ the lock-in time constant (300 ms). Three data streams are acquired for each block of the reference and sample measurements. The three measurements are normalized to the mean value of the baseline of the first measurement, after which the baseline is removed from the interferograms. Prior to Fourier-transforming, the interferograms are apodized using a triangular window function and then averaged together. For the reflectance measurements an additional step is needed in order to consider the diffraction effect of the aluminum mask used to hold the sample in place. A set of three interferograms with only the aluminum mask is acquired and then averaged. The resulting interferograms are subtracted from both the reference and sample measurements prior to apodization. The reflectance and transmittance of the sample are obtained from the ratio between the sample and reference spectra.

Furthermore, the refractive index is independently obtained by measuring the shift of the zero path difference (ZPD) when a thin sample of the lossy material is placed in one of the two arms, according to the following equation:

$$\Delta x_{ZPD} = d(n-1)$$

A thin layer with an average thickness of 0.82 ± 0.12 mm of carbon-loaded $(10\,\%)$ STYCAST 2850FT is used for this measurement. The measured ZPD shift is 0.88 ± 0.01 mm as shown in Fig.6, resulting in a value of $n = 2.07 \pm 0.16$. The loss tangent of the thin layer is estimated by using a six parameters Monte Carlo fit[9] of the transmittance at $0°$ and $30°$ of incidence angles over the $175 - 500$ GHz frequency band. Due to the high roughness of the sample and the non-uniform thickness, the fit does not accurately reproduce the measured profile, resulting in an average estimation of the loss tangent, which is $tan\delta = 0.151 \pm 0.010$.

The test prototype with ARC is a 60×60 mm^2 plate based on a mixture of STYCAST 2850FT $(90\,\%)$ and carbon black $(10\,\%)$. Fig.7 shows the measured reflectance for two incidence angles $(22.5°$ and $45°)$. The reflectance is less than 1% above ~ 200 GHz despite the generalized deformation of the pyramid shape, even if predictably worse than expected from the nominal geometry simulation. In particular, we attribute the excess reflectance below 250 GHz to the different aspect ratio of the manufactured pyramids, due to the observed truncation of their tips and the filling at the base.

The prototypes diffuse and specular reflection is measured also using the TOPtica reflectometry system. The
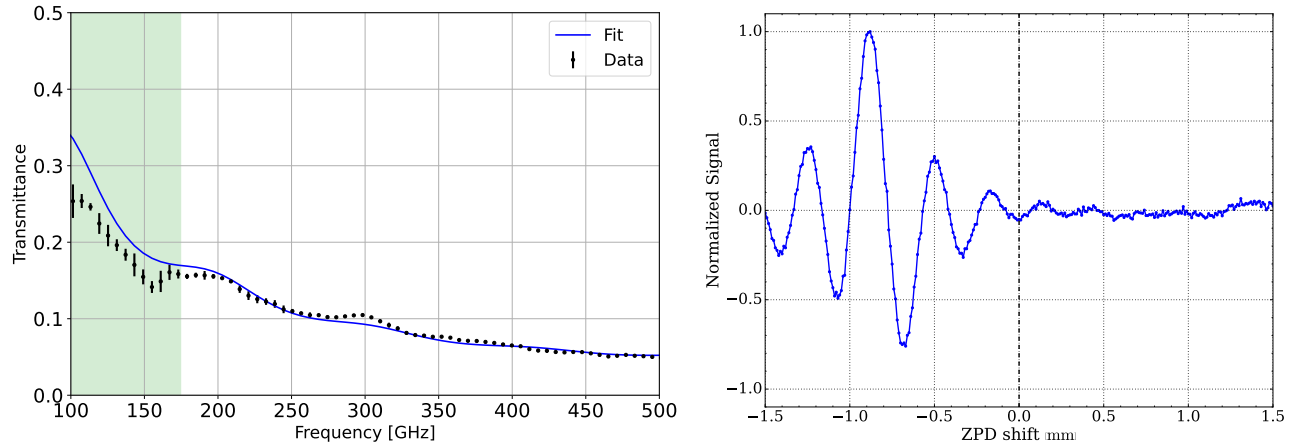
Figure 6. Left: The measured transmittance of a thin layer (820 µm) of carbon-loaded (10 %) STYCAST 2850FT prototype at 0°. The blue curve represent the best fit as described in the text. The green shadow is the data region excluded from the fit. Right: The interferogram shift when the thin sample is inserted in the one of the two arms of the DFTS.
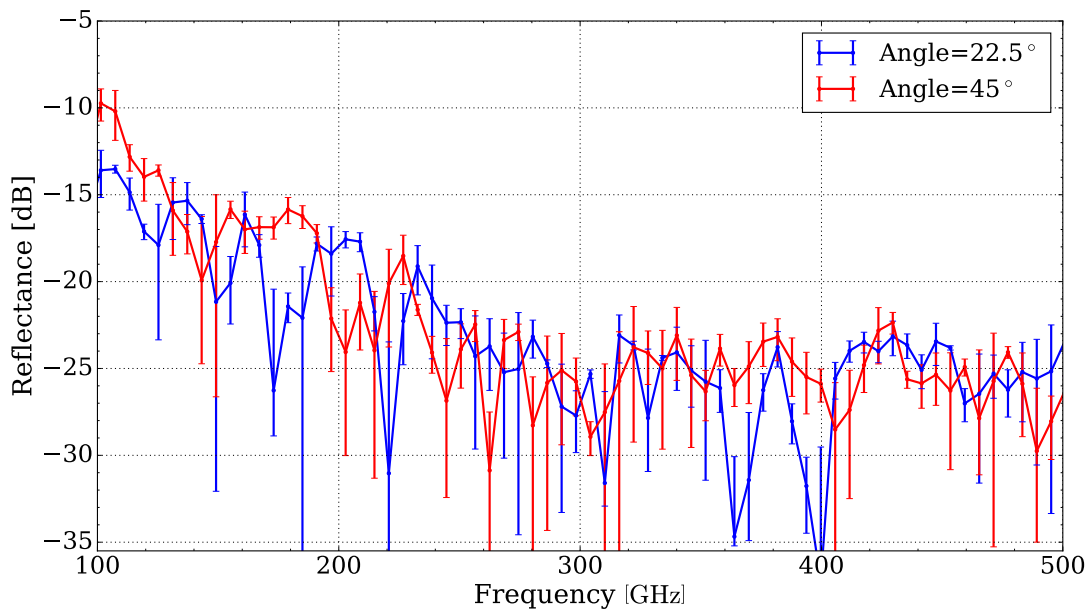

Figure 7. The reflectance of the carbon-loaded (10 %) STYCAST 2850FT prototype for 22.5° and 45° incidence angles.

specular reflection measurement is performed with Tx and Rx modules mirrored across the axis normal to the incidence place. The diffuse reflection measurement is performed by scanning with the receiver module across a number of angles to measure the amount of non-specular reflection. Fig.8 shows the specular reflection of the STYCAST prototype at different incidence angles and compared with other commercial solution (Eccosorb AN72, Eccosorb HR10 and TKRAM). The measurements obtained with the coherent setup are in agreement with those obtained with the DFTS. The Eccosorb HR10 and the TKRAM exhibit a lower reflectance in comparison to the STYCAST prototype. However, these solutions fail to meet the other specified requirements. In particular, the Eccorsorb HR10 is not qualified or qualifiable for space applications, while the TKRAM has a high density, exceeding the mass budget allocated for the absorbers and it lacks a customizable shape. Fig.9 shows the diffuse reflection of the STYCAST prototype at different incidence angles and compared again with Eccosorb AN72, Eccosorb HR10 and TKRAM.
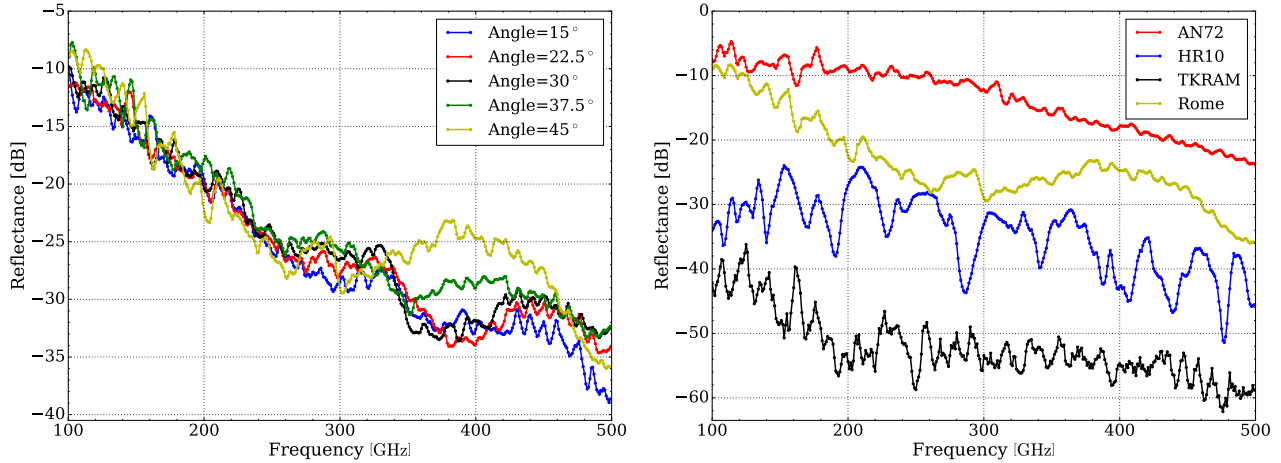
Figure 8. Left: The specular reflectance of the carbon-loaded STYCAST prototype for incidence angles from $15°$ to $45°$ with a step size of $7.5°$. Right: A comparison of the specular reflectance at $45°$ between the carbon-loaded STYCAST prototype (Rome) and some commercial alternatives as Eccosorb AN72, Eccosorb HR10 and TKRAM.
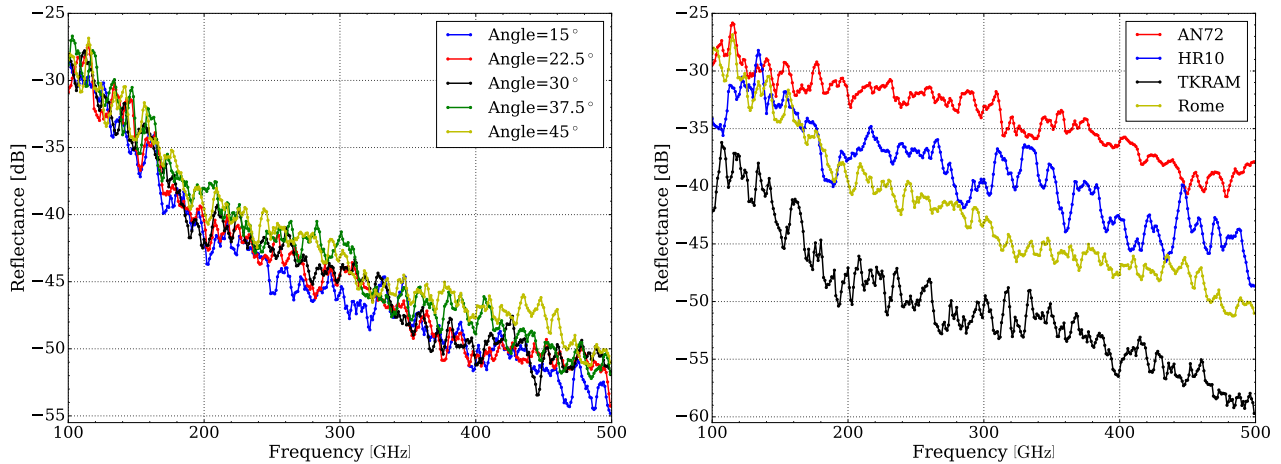

Figure 9. Left: The diffuse reflectance of the carbon-loaded STYCAST prototype for incidence angles from $15°$ to $45°$ with a step size of $7.5°$. Right: A comparison of the diffuse reflectance at $45°$ between the carbon-loaded STYCAST prototype (Rome) and some commercial alternatives as Eccosorb AN72, Eccosorb HR10 and TKRAM.

5. CONCLUSION

We present preliminary results of the development of the *LiteBIRD* MHFT absorbers. We have designed and simulated an anti-reflection coating based on a 3D square-based pyramids with a side length of 0.6 mm and a height of 1.5 mm. The simulated reflectance of this design meets the current 1% requirement for a wide range of incidence angles. A further simulation was conducted which included deviations from the nominal geometry in order to account for any shape distortions that might occur during the manufacturing process.

A manufacturing process for prototypes was developed using different recipes and a three stage molding process. A prototype was fabricated using a mixture of carbon-loaded (10%) STYCAST 2850FT. SEM imaging of the prototype revealed distortions from the nominal geometry of the pyramids, with deviations of approximately $\sim 40\,\mu$m on the side and $\sim 300 - 500\,\mu$m in height.

Refractive index ($n = 2.07 \pm 0.16$) and transmittance measurements at $0°$ were performed on a thin layer prototype fabricated with the same loaded mixture. The measured transmittance was fitted with the model, resulting in a loss tangent of $tan\delta = 0.151 \pm 0.010$.

The specular reflectance was measured using two independent setups, resulting below 1% for frequencies above

200 GHz, while it did not meet the requirement at lower frequencies due to the general deformation of the pyramidal shape. A refined manufacturing process is currently under investigation to improve the performance. A modification of the mixture recipe which include the addition of silica powder or alumina in order to match the thermal expansion coefficient to that of the aluminum substrate is also under development. In addition, the thermo-mechanical characterization of the prototypes and the definition of an attachment strategy on the wall of the optical tube will be initiated soon.

ACKNOWLEDGMENTS

REFERENCES

[1] LiteBIRD Collaboration, Allys, E., Arnold, K., Aumont, J., Aurlien, R., Azzoni, S., Baccigalupi, C., Banday, A., Banerji, R., Barreiro, R., et al., "Probing cosmic inflation with the litebird cosmic microwave background polarization survey," *Progress of Theoretical and Experimental Physics* **2023**(4), 042F01 (2023).

[2] Savini, G. et al., "Using Zemax Programming Language and API as a method to perform parametric ghost analysis, chromatic aberrations and baffle thermal loading on the Litebird Medium and High Frequency Telescopes," in [*Space Telescopes and Instrumentation 2024: Optical, Infrared, and Millimeter Wave*], **13092-204**, International Society for Optics and Photonics, SPIE (2024).

[3] Mather, J. C., Fixsen, D., Shafer, R., Mosier, C., and Wilkinson, D., "Calibrator design for the cobe* far infrared absolute spectrophotometer (firas)," *The Astrophysical Journal* **512**(2), 511 (1999).

[4] Gudmundsson, J. E., Gallardo, P. A., Puddu, R., Dicker, S. R., Adler, A. E., Ali, A. M., Bazarko, A., Chesmore, G. E., Coppi, G., Cothard, N. F., et al., "The simons observatory: modeling optical systematics in the large aperture telescope," *Applied Optics* **60**(4), 823–837 (2021).

[5] Wollack, E., Fixsen, D., Henry, R., Kogut, A., Limon, M., and Mirel, P., "Electromagnetic and thermal properties of a conductively loaded epoxy," *International Journal of Infrared and Millimeter Waves* **29**, 51–61 (2008).

[6] Rostem, K., Cimpoiasu, E., Helson, K., Klassen, A., and Wollack, E., "Specific heat of epoxies and mixtures containing silica, carbon lamp black, and graphite," *Cryogenics* **118**, 103329 (2021).

[7] Wollack, E. J., Kinzer, R. E., and Rinehart, S. A., "A cryogenic infrared calibration target," *Review of Scientific Instruments* **85**(4) (2014).

[8] Lamagna, L., Basilicata, M., Occhiuzzi, A., Columbro, F., Coppolecchia, A., D'Alessandro, G., Bernardis, P. d., Masi, S., Mele, L., Paiella, A., et al., "A testbed for modeling validation and characterization of quasi-optical elements in microwave receivers," *Journal of Low Temperature Physics* **209**(5), 1272–1279 (2022).

[9] Columbro, F., Occhiuzzi, A., Lamagna, L., Mele, L., de Bernardis, P., Masi, S., Piacentini, F., and Pisano, G., "Broadband spectral characterization of lossy dielectrics for mm/submm optical applications," in [*Space Telescopes and Instrumentation 2022: Optical, Infrared, and Millimeter Wave*], **12180**, 885–895, SPIE (2022).

[10] Pisano, G., Ng, R., Zhu, C., Tucker, C., and Ade, P., "Multi-octave anti-reflection coating for polypropylene-based quasi-optical devices," in [*Millimeter, Submillimeter, and Far-Infrared Detectors and Instrumentation for Astronomy IX*], **10708**, 787–793, SPIE (2018).

[11] Chuss, D. T., Rostem, K., Wollack, E. J., Berman, L., Colazo, F., DeGeorge, M., Helson, K., and Sagliocca, M., "A cryogenic thermal source for detector array characterization," *Review of Scientific Instruments* **88**(10) (2017).

[12] Xu, Z., Chesmore, G. E., Adachi, S., Ali, A. M., Bazarko, A., Coppi, G., Devlin, M., Devlin, T., Dicker, S. R., Gallardo, P. A., et al., "The simons observatory: metamaterial microwave absorber and its cryogenic applications," *Applied Optics* **60**(4), 864–874 (2021).

[13] Columbro, F., de Bernardis, P., Lamagna, L., Masi, S., Paiella, A., Piacentini, F., and Pisano, G., "A polarization modulator unit for the mid-and high-frequency telescopes of the litebird mission," in [*Space Telescopes and Instrumentation 2020: Optical, Infrared, and Millimeter Wave*], **11443**, 1113–1128, SPIE (2020).

[14] Columbro, F. et al., "Development of the polarization modulator and multi-mode receivers for the search of cmb polarization," *Memorie della Società Astronomica Italiana Journal of the Italian Astronomical Society* , 11 (2021).